PAN
POLSKA AKADEMIA NAUK

M&MS

MODEL BASED MONITORING OF HYPOTHERMIC PATIENTS

Michael Schwarz[1], Claudia Heilmann[2], Martin W. Krueger[3], Uwe Kiencke[1]

1) Universität Karlsruhe (TH)*, Institut für Industrielle Informationstechnik, Hertzstrasse 16, 76187 Karlsruhe, Germany*
(✉ schwarz@iiit.uni-karlsruhe.de, +49 721 608-4521, kiencke@iiit.uni-karlsruhe.de)
2) Universitätsklinikum Freiburg Herz-Kreislauf Zentrum, Elsässer Strasse 2n, 79110 Freiburg, Germany
(claudia.heilmann@uniklinik-freiburg.de)
3) Universität Karlsruhe, Institut für Biomedizinische Technik, Kaiserstrasse 12, 76128 Karlsruhe, Germany
(martin.krueger@ibt.uni-karlsruhe.de)

Abstract

In open heart surgery the patient is connected to a heart-lung machine which pumps and oxygenizes the blood. The body core temperature is reduced by cooling the blood in a heat exchanger to reduce oxygen consumption of the tissues and so protect organs from hypoxia. Monitoring of vital parameters is crucial for safety of the patient. However, only little information is available from direct measurement. Models of haemodynamics and heat exchange in the human body are presented in this paper which provide the perfusionist with detailed data on blood flow and temperature in regions of the body which cannot be accessed by measurement devices. Simulation is performed on a real-time hardware platform which receives measured signals from the heart-lung machine via a serial interface.

Keywords: biomedical engineering, human modelling, real-time application.

1. Introduction

Coronary disease and acquired valvular heart disease are widespread in the industrial nations. Surgical treatment of such diseases requires initiation of cardioplegia to stop heartbeat during the procedure. Circulation is sustained by the arterial pump of a heart-lung machine. Blood is drained from the venae cavae and is oxygenized and cooled in the extracorporeal circuit before it re-enters the aorta. Depending on the type of operation certain areas of the body may be excluded from perfusion and suffer hypoxia. Especially the brain and the spinal cord are prone to irreversible damage. Tissue can be protected by hypothermia since reducing body core temperature by 1 K lowers the metabolic rate and oxygen consumption by ca. 7% (Arrhenius equation) [1]. The degree of hypothermia reaches from mild (32-36 °C) to deep (15-28 °C) hypothermia depending on the type of operation. Monitoring of vital parameters is an important safety aspect during extracorporeal circulation. However, standard monitoring includes only measurement of the arterial pressure in the radial artery, central venous pressure, arterial and venous blood temperature in the extracorporeal circuit, body core temperature at two locations, determination of activated clotting time and blood gas analysis.

Safety of the procedure is determined by perfusion and temperature of tissue sensitive to hypoxia. Information on these parameters is not accessible by direct measurement but can be provided by simulation models. Requirements for such models are easy patient-specific parametrization and real-time computability.

A one-dimensional linear model of the haemodynamics is introduced in Section 2. It is based on Avolio's model of the systemic arteries [2] and extended by important structures in the brain, a stenosis model and controllers to simulate circulatory regulation. Section

3 explains an anatomical six cylinder temperature model which is based on Pennes' bioheat equation [3]. Flow rates from the haemodynamics model are used to determine the perfusion rates in the tissues (see Fig. 1). This new approach is crucial to simulate cooling and rewarming of the tissue. Technical realization is explained in Section 4 and simulation results are discussed in Section 5.

2. Arterial haemodynamics

During extracorporeal circulation blood is led in the aorta and transported to the tissues via arteries, arterioles and capillaries. Real-time simulation of flux in such a complex system requires a model with low computational effort. Avolio [2] published one of the most established models of the systemic arteries. It is a linear 1D model based on the transmission line approach and therefore nowadays real-time computable. We extended the model by additional arteries in the brain which is crucial to simulate cerebral blood flow under extracorporeal circulation.
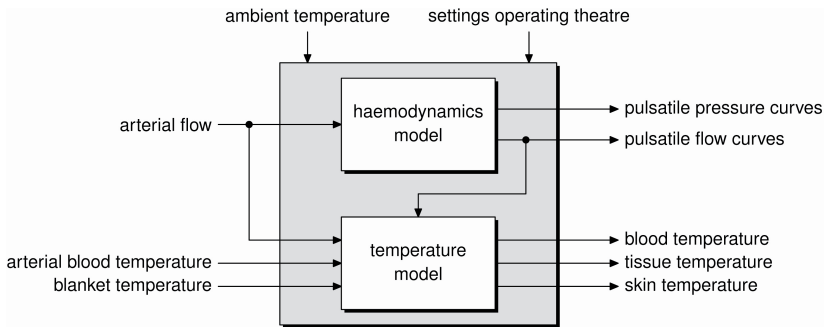

Fig. 1. Structure of the model.

Several authors have published models of cerebral haemodynamics including nonlinear 1D models [4, 5, 6], 2D models [7] and 3D models [8, 9]. These approaches are more complex and require more computational effort. Furthermore, these models do not consider overall circulation and are therefore not suitable for our objective. However, they can serve as a reference to evaluate the presented model (see Section 5).

2.1. The transmission line approach

The basic equations of the transmission line approach are derived from the Navier-Stokes equation and the continuity equation. Pulsatile flow, curvature of the vessels and the numerous bifurcations of the arterial system cause deviations from a parabolic velocity profile. The transmission line approach is an idealization which assumes a one-dimensional laminar flow in a long, cylindrical, elastic tube. Gravity is neglected and blood is considered a Newtonian fluid. The resulting flow equations correspond to the equations of an electrical transmission line:

$$-\frac{\partial p}{\partial z} = L' \cdot \frac{\partial q}{\partial t} + R' \cdot q$$

$$-\frac{\partial q}{\partial z} = C' \cdot \frac{\partial p}{\partial t},$$

(1)

where: p – pressure, q – flow, t – time, z – flow direction. The coefficients R', L' and C' are the resistance (according to Poiseuille's law), inertance and compliance per unit length, respectively. They are determined by characteristics of the fluid (density ρ, dynamic viscosity η) and of the vessel (radius r_0, Young's modulus E and thickness d of the walls):

$$R' = \frac{8\eta}{\pi r_0^4}, \, L' = \frac{\rho}{\pi r_0^2}, \, C' = \frac{3\pi r_0^3}{2Ed}. \tag{2}$$

Pulsatile flow and pressure curves in an elastic vessel can be simulated with the transmission line equations for given boundary conditions.

Discretization of the partial differential equations with respect to z leads to state-space representations of a short tube of length Δz. They approximate the transmission line if the length of the tube is sufficiently short which means that Δz is small compared to the shortest wave length:

$$\Delta z \ll \lambda_{min} \approx \frac{1}{f_{max} \cdot \sqrt{L'C'}}, \tag{3}$$

where: $f_{max} = 15\,\text{Hz}$ can be considered the frequency of the maximum relevant harmonic in physiological flow and pressure signals [2, 10].

Fig. 2 shows the electrical analogons of four different discrete representations of the transmission line. All of them approximate a short tube. Such quadripoles can be connected applying Kirchhoff's law to model complex systems of vessels. State-space representations can be found for arbitrary topologies which comprise *e.g.* bifurcations and anastomoses [11]. The adequate type of quadripole to model a segment is determined by the given boundary conditions (shaded grey in Fig. 2), *e.g.* given input pressure and output flow at a bifurcation requires the standard quadripole.
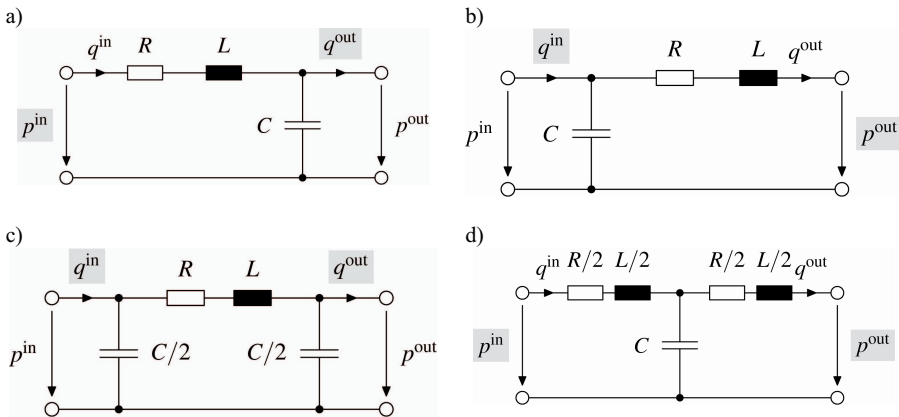

Fig. 2. Discretization of the transmission line. a) Standard quadripole; b) Inverse quadripole; c) π quadripole; d) T quadripole.

2.2. The Avolio model

In 1980 Avolio published a transmission line model which maps the systemic arteries to a tree-like topology of 128 segments [2]. The structure of the model is shown in Fig. 3. Nomenclature and parametrization of the segments are given in [2].

Smaller vessels which are not included in Avolio's topology, especially the arterioles and capillaries, are modelled by "grounded" terminal impedances. They can be determined by one of the following strategies.

DC models aim at a correct representation of the mean flow in the individual branches of the arterial system. They are useful to simulate blood flow to the organs and to assess the risk of hypoxia in vital organs. Resistors are used as terminal impedances. Their initial values can be determined for given physiological flow rates in the branches of the model and a given total peripheral resistance (TPR). The TPR is the quotient of the pressure drop across the systemic vessels and the cardiac output (or the flow rate of the arterial pump).

AC models neglect the mean flow rates and try to simulate the pulsatile flow and pressure curves accurately. Information on pulsatility is useful during extracorporeal circulation as the pressure peaks influence microcirculation [12, 13]. The terminal impedances of AC models are determined such that physiological reflection coefficients:

$$\Gamma^t = \frac{Z^t - Z_0}{Z^t + Z_0} \tag{4}$$

are obtained, where Z^t is the terminal impedance and Z_0 is the characteristic impedance. Typical terminal impedances are resistors (*e.g.* [2]) or so-called three-element Windkessel models (*e.g.* [14]). Resistors lead to a constant reflection coefficient for all frequencies, the Windkessel model can be parameterized such that a matched line ($Z^t = Z_0$, $\Gamma^t = 0$) is obtained for $f \to \infty$. Wave reflection is damped for high frequencies in this case.

We apply a DC approach in our model and apply a low-pass filter to the input flow signal hereby damping high-frequency oscillations in the pulsatile curves caused by non-physiological reflection coefficients.
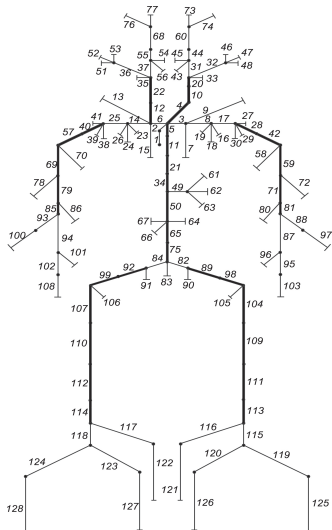

Fig. 3. Topology of the Avolio model [2] (with minor corrections in numbering); thick lines mark central vessels of the temperature model.
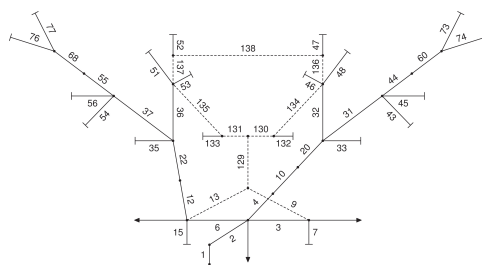

Fig. 4. Topology of the head with integrated Circle of Willis (dashed segments).

2.3. Circle of Willis

The brain is particularly vulnerable to hypoxia. The human body provides a system of alternative pathways leading oxygenized blood to the cerebral arteries. These pathways form a ring-like structure, the Circle of Willis, which is not considered in the Avolio model. Fig. 4 shows an extended topology of the head which includes the collateral routes. The afferent arteries of the Circle of Willis are the internal carotid arteries (segments 32, 36) and the vertebral arteries (9, 13). The vessels to be supplied are the anterior (47, 52), middle (46, 53) and posterior (132, 133) cerebral arteries. The collateral pathways are provided by the anterior (138) and posterior (134, 135) communicating arteries. Geometrical parameters of the additional segments are given by Schwarz *et al.* [11]. The short length of the anterior communicating artery implies that Poiseuille's law is not valid for this segment. Moore *et al.* [8] found that flow resistance is approximately nine times higher.

The Circle of Willis becomes particularly important in case of an asymmetrical perfusion of the afferent arteries which may be caused by stenoses. Therefore, this extension of the Avolio model is crucial to predict cerebral flow correctly. The complex structure can be modelled by inserting the adequate quadripole for each segment (cf. Section 2.1). The resulting electrical circuit is shown in [11]. We also consider anatomical variations with hypoplastic arteries which are discussed by Alastruey *et al.* [4].

2.4. Stenosis model

A stenosis is an abnormal narrowing in a vessel often caused by atherosclerosis. It can be located and assessed by preoperative sonography. The severity of a stenosis:

$$S = 1 - \frac{r_{sten}}{r_0} \tag{5}$$

is defined by the radius r_{sten} in the stenosed part of the vessel and the radius r_0 without a stenosis. Stenoses in the internal carotid arteries may impact cerebral flow. They are a common comorbidity of patients with cardiac disease. Carotid stenoses are normally asymptomatic up to $S = 80\%$ due to the collateral pathways in the Circle of Willis and vasodilation of the distal arterioles. Moreover, an increase in the diameter of the communicating arteries may occur as a long-term effect.

The electrical analogon of a stenosed vessel is shown in Fig. 5. It is divided into a proximal part before the stenosis, a stenosed part and a distal part after the stenosis. The proximal and distal parts are standard quadripoles whereas the stenosed part is modelled as an increased flow resistance due to the diminished diameter:

$$R_{sten} = \frac{8\eta \Delta z_{sten}}{\pi r_0^4 (1-S)^4}, \tag{6}$$

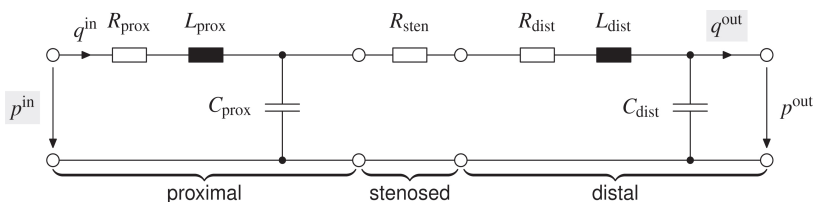where Δz_{sten} is the length of the stenosis.

Fig. 5. Electrical analogon of a stenosed vessel.

The distal terminal resistors are varied in the initialization phase of the model if a stenosis is present in order to simulate vasomotor effects which contribute to a compensation of the stenosis. The simulation results show insufficient local cerebral perfusion depending on the severity of the stenosis and the anatomical variant of the Circle of Willis.

2.5. Circulatory regulation

Variation of the terminal resistors during simulation allows consideration of mechanisms of circulatory regulation which influence arterial pressure and regional blood flow. Measurement of arterial pressure at the radial artery is included in standard monitoring. The measured value is used to adapt the simulated pressure by varying the total vascular resistance in a control loop (cf. [15]).

Blood flow in the brain and the kidneys is constant under physiological conditions even if arterial pressure varies. This autoregulation mechanism is not active in the kidneys under hypothermia, where renal blood flow depends on the flow of the arterial pump and the arterial pressure [16]. Cerebral autoregulation depends on pH of blood. A high partial pressure of carbon dioxide causes a dilatation of the cerebral arteries and thus a significant increase in cerebral blood flow [13]. We assume an intact autoregulation in the following considerations.

The response of the autoregulatory system to an arterial pressure drop has been investigated in a clinical study by Newell *et al.* [17] (see Fig. 6a). The results have been used to develop models of the control mechanisms [7, 8, 9, 18]. An integral controller is applied in the presented model to approximate the observed dynamic behaviour:

$$\frac{d\beta_i^{auto}}{dt} = -0.1\,\text{ml}^{-1} \cdot (q_i^{cap} - q_i^{ref}), \tag{7}$$

where: q_i^{cap} is the current flow in the controlled branch and q_i^{ref} is the reference flow. The coefficient β_i^{auto} is used to vary the terminal resistance: $R_i^{auto} = R_i / \beta_i^{auto}$. The controller gain has been such that a realistic time constant results for the response (see Fig. 6a).

Autoregulation is constricted by the limits of vascular constriction and dilatation. Cerebral flow is maintained constant only if arterial pressure ranges between 75 and 175 mmHg [19]. Therefore, β_i^{auto} is limited to $0.53 \le \beta_i^{auto} \le 1.54$ (Fig. 6b).

a) Autoregulation response after pressure drop
from 100 to 80 mmHg:
— model, Newell *et al*. [17]

b) Range of autoregulation:
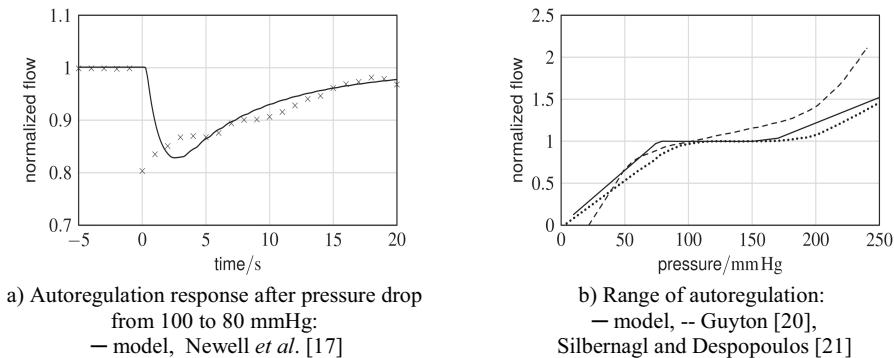— model, -- Guyton [20],
Silbernagl and Despopoulos [21]

Fig. 6. Cerebral autoregulation: comparison between simulation and reference curves.

3. Heat transfer in the human body

Heat balance of the human body is determined by metabolic heat production, heat transfer via blood and conduction, and heat loss via lung and skin. Thermoregulation aims at maintenance of a constant core temperature of approximately 37 °C by controlling skin blood flow, sweating and shivering.

Patients in open heart surgery are put in hypothermia by perfusion with cold blood and application of heating-cooling blankets to reduce oxygen consumption. If the core temperature is reduced by 10 K the metabolic rate drops by a factor 2-2.5 [1]. Drug induced relaxation of the skeletal muscles inhibits heat production by shivering. Furthermore, anaesthesia increases the thresholds for sweating and vasodilation by 1 K and diminishes the vasoconstriction threshold by 2-4 K. The total effect is an increased neutral zone of thermoregulation [22, 23].

In order to model heat transfer in the human body, its shape is often approximated by simple geometric shapes [24, 25, 26, 27]. The presented model consists of six elliptic cylinders which represent the head, torso, arms and legs. The dimensions of the cylinders are adapted to the patient's height and mass. Each cylinder consists of a central artery and vein, tissues and a skin layer (Fig. 7).

3.1. Central vessels

A central blood pool is a common approach to describe convective heat transport in temperature models of the body. Fiala *et al.* [24] provide additional countercurrent heat exchangers to account for direct heat transfer between vessels. However, the large temperature differences between blood and tissue which occur in hypothermic patients require a more detailed approach.

A central artery and vein represent large vessels in each domain, *e.g.* the brachial arteries in the arms. Their parametrization is derived from the Avolio model (see Fig. 3). The artery transports blood along the cylinder's axis and supplies the surrounding tissue. Capillary blood is collected in the central vein and transported back. Moreover, conductive heat transport via the vessels' walls is considered which results in realistic axial temperature gradients in the extremities.
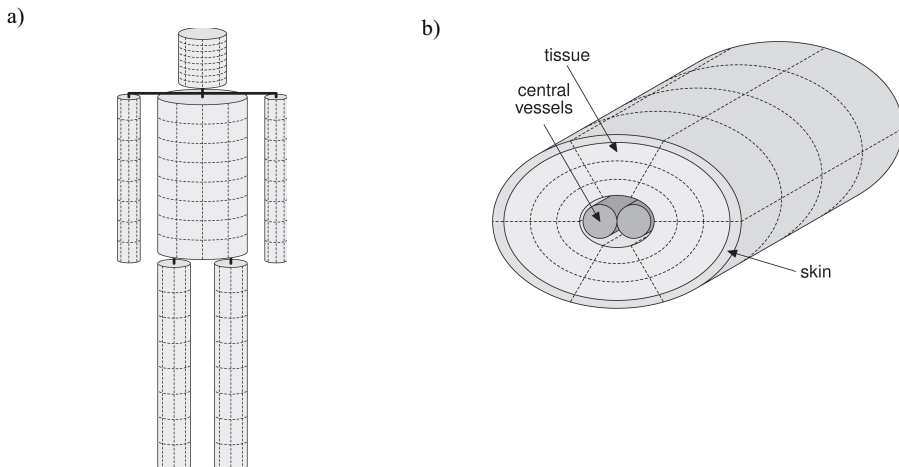

Fig. 7. Cylinder model. a) Shape of the body; b) Profile of a cylinder.

3.2. Tissue

The tissues of the body differ in terms of physical and physiological properties. The thermal conductivity λ_{tis} determines conductive heat transfer. Density ρ_{tis} and specific heat capacity c_{tis} influence the capability of storing thermal energy. Local heat production depends on the metabolic rate $\dot{w}_{met}$ and effectivity of cooling or heating by circulating blood is determined by the perfusion rate $\dot{v}_{bl}$.

Heat transfer is derived from Pennes' bioheat equation [3]:

$$\rho_{tis} \cdot c_{tis} \cdot \frac{\partial T_{tis}}{\partial t} = \text{div}(\lambda_{tis} \cdot \text{grad}\, T_{tis}) + \dot{w}_{met}(T_{tis}) + \rho_{bl} \cdot c_{bl} \cdot \dot{v}_{bl} \cdot (T_{art} - T_{tis}), \tag{8}$$

where: T_{art} – arterial temperature, T_{bl} – blood temperature, ρ_{bl} – density of blood and c_{bl} – specific heat capacity of blood. The coefficient β accounts for countercurrent heat exchange between larger vessels; $\beta = 1$ means total thermal equilibration between arterial blood and tissue.

In many cases a simple core-shell structure is sufficient for temperature models with physiological blood circulation. However, the local cooling rate depends on the perfusion rate of the tissue when perfusion with cold blood is applied. Therefore a more detailed structure is required. We distinguish between right and left brain, brain stem and cranial bone in the skull. Heart, lung, gastro-intestinal tract, kidneys and liver are considered in the torso. Further volume segments are assigned to bone, subcutaneous fat, musculature and several "composite tissues". Shape and location of the organs are derived from a classified Visible Human dataset [28, 29] by adapting the structure manually to the cylinder grid (Fig. 8). Spatial discretization is a compromise between precision and computational effort. The perfusion rate is determined from the haemodynamics model assigning capillary flow to the corresponding domain in the temperature model.
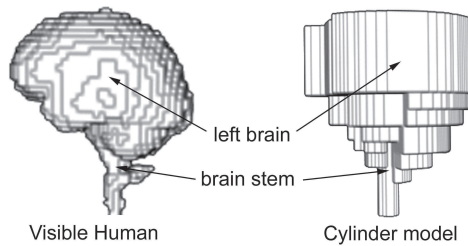

left brain

brain stem

Visible Human   Cylinder model

Fig. 8. Shape of the brain.

3.3. Skin layer and thermoregulation

Heat transfer in the skin is also derived from the bioheat equation. However, perfusion of the skin is controlled by thermoregulation mechanisms. Several models of thermoregulation have been developed over the past decades, *e.g.* Stolwijk and Hardy [26], Gordon *et al.* [25]. Fiala *et al.* [30] presented empirical formulae for vasoconstriction, vasodilation and the resulting skin perfusion which are based on numerous clinical studies. This approach has been adapted for the presented model to consider the increased neutral zone in anaesthetized patients.

3.4. Heat loss

The individual situation of the patient in the operating theatre has to be considered to estimate heat loss of the body to the environment. The back side of the patient normally is in contact with the operating table or a heating-cooling blanket. The front side is covered by surgical drapes while only the surgical field and the face are directly exposed to the surrounding air. Hence, four cases of boundary conditions have to be distinguished. The parametrization of the model allows assigning the appropriate boundary condition to each segment of the skin.

In each case heat exchange via radiation, conduction and evaporation has to be considered. A model for heat transport through clothing [27] is used to estimate heat flow density if the skin is covered by a surgical drape.

4. Technical realization

The complete model has been implemented on a rapid prototyping hardware for real-time simulation. The hardware is connected to the heart-lung machine via a serial interface to pick up measurement signals and settings of the machine. Simulation is performed on two Power PC 750 processors (clock rate 480 MHz). The processor boards provide 1 MB of L2 cache and 128 MB of RAM each.

The haemodynamics model is simulated with a Runge-Kutta solver (turnaround time: 0.13 ms). The finite volume method is applied to discretize the bioheat equation of the temperature model. Turnaround time is 6.7 ms using an Euler solver with a spatial discretization of approximately 8,500 volume elements.

A graphical user interface allows parametrization of the model as well as real-time visualization of the simulation results. Simulation starts when total cardiopulmonary bypass is established. Look-up tables for an initial temperature field were created from simulations of passive cooling before initiation of the bypass. The model is automatically initialized with an appropriate temperature field which is derived from measured core temperatures (e.g. nasopharyngeal and rectal temperature).

5. Results and discussion

5.1. Cerebral haemodynamics

The presented haemodynamics model considers the systemic arteries of the whole body. Particularly a precise prediction of cerebral blood flow is of vital importance for the safety of the patient. Three-dimensional models of the Circle of Willis show a high accuracy but require much computational effort. Moore *et al.* [8] published simulation results from a 3D model. They show the mean blood flow in several arteries after a pressure drop of 20 mmHg in the right internal carotid artery. Their model accounts for vasodilation caused by autoregulation of the brain. Fig. 9 approves the results of the transmission line model comparing them to Moore's results.

The observed discrepancies for the larger cerebral vessels are less than 25%. Also the communicating arteries show little absolute deviations. The transmission line model is therefore assumed to allow for sufficient assessment of the cerebral perfusion. Statements on reliability of the model will require clinical studies employing transcranial Doppler sonography.
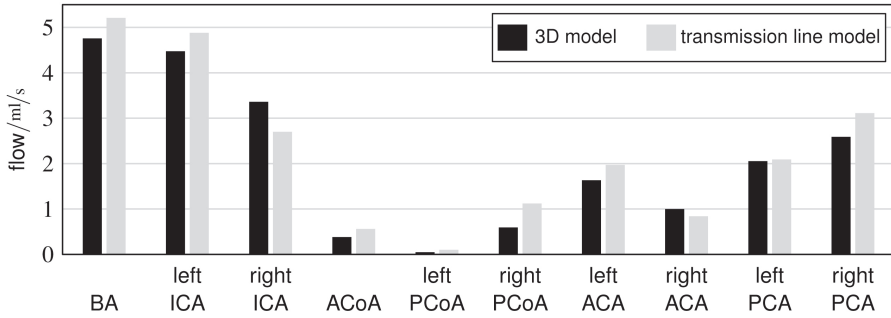
Fig. 9. Comparison of Moore's 3D model [8] and the transmission line model: flow in basilar artery (BA), internal carotid arteries (ICA), anterior (ACoA) and posterior (PCoA) communicating arteries, anterior (ACA) and posterior (PCA) cerebral arteries after a pressure drop of 20 mmHg in the right internal carotid artery.

5.2. Temperature model

Measurement signals from real open-heart surgeries are used to evaluate the temperature model. Data recording starts when total cardiopulmonary bypass is initiated. Passive cooling already led to hypothermia by this time in the presented example. Sample time of the signals is 10 s, measuring accuracy of the temperature values is 0.1 K. Standard monitoring includes measurement of the arterial temperature, the venous temperature and two core temperatures. The arterial temperature is the temperature of the blood which enters the body and is required as an input signal to the model.

The venous temperature is the temperature of the blood which leaves the body and flows back to the heart-lung machine. It is determined by the heat exchange between arterial blood and tissue and so approximately represents a weighted sum of the tissue temperatures, where the weighting factors correspond to the local perfusion rates. Fig. 10a compares the measured and simulated signal of the venous temperature during a mitral valve replacement. The curves converge within the first 15 min. Afterwards, deviations are less than 0.2 K (apart from minor fluctuations in the measured signal). The initial deviations are caused by the estimation of the initial temperature field described in Section 4. Increasing experience will enable to improve the estimation and reduce the deviations by this means.

The rectal temperature is measured in the vicinity of weakly perfused tissue which results in slow changes in temperature. Therefore, a good estimation of the initial temperature is required. Fig. 10b shows that again deviations between measured and simulated curve are less than 0.2 K.

The measured temperature in the pulmonary artery (Fig. 10c) shows more pronounced fluctuations which are due to the proximity to the surgical field and are caused *e.g.* by the influence of cold cardioplegia. They only affect local blood temperature but not more remote tissue and should therefore not be reproduced by the model. Due to stronger perfusion the temperature signal follows the arterial temperature more quickly than the rectal temperature, especially during rewarming. This behaviour is also represented by the simulated curve.

The brain temperature cannot be measured directly but is available from the model. The simulated curve is shown in Fig. 10d. Temperatures in both hemispheres are identical due to assumed symmetrical perfusion for this patient.

a) Blood temperature:
— venous (measured), -- venous (simulated),
— arterial (measured, input signal*)*

b) Rectal temperature:
— measured, -- simulated

c) Temperature in pulmonary artery:
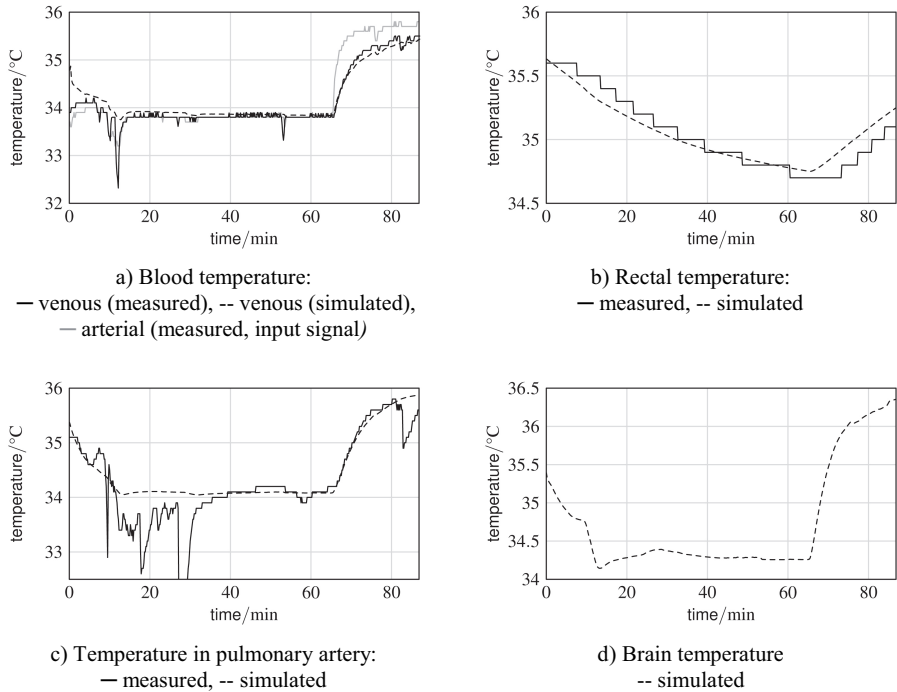— measured, -- simulated

d) Brain temperature
-- simulated

Fig. 10. Simulation results of a mitral valve replacement in hypothermia.

6. Conclusions

Real-time models of haemodynamics and heat transfer in the human body are capable of extending information on hypothermic patients in cardiac surgery significantly.

Our simulation system contains a detailed model of the vascular system including the Circle of Willis. This intracerebral network can be adapted for its anatomical variations which is necessary to predict cerebral flow adequately. Real-time computability is achieved by the transmission line approach. The simulated arterial pressure is adapted to the measured value.

Cerebral autoregulation is realized by integral controllers in each cerebral branch of the model. Existing stenoses are modelled by an increased flow resistance in the affected vessel.

Simulation of temperature fields is based on an anatomical cylinder model. The shape and location of the organs have been derived from a classified Visible Human data set. Calculation of heat transfer in the tissue is based on Pennes' bioheat equation. The model considers varying perfusion of the tissues during the surgical procedure as well as the influence of thermoregulation on skin perfusion. The setup allows specifying the size and location of surgical drapes and heating-cooling blankets to estimate heat loss of the body. By this means temperature fields in unaccessible regions like brain or spinal cord can be simulated.

Simulation is intended to enhance safety for patients during extracorporeal circulation. Simulation results of the haemodynamics model have been successfully evaluated comparing them to published results of a 3D simulation model. Simulated temperature values could be verified with measured curves from heart surgery. The combined model has been implemented on a real-time hardware and is ready for comprehensive clinical evaluation.

Acknowledgements

References

[1] R.J. Tschaut: *Extracorporeal circulation in theory and practice*. Pabst Science Publishers, 1999. (in German)

[2] A.P. Avolio: "Multi-branched model of the human arterial system". *Med Biol Eng Comput*, vol. 18, 1980, pp. 709-718.

[3] H.H. Pennes: "Analysis of tissue and arterial blood temperatures in the resting human forearm". *J. Appl. Physiol.*, vol. 1, no. 2, 1948, pp. 93-102.

[4] J. Alastruey, K.H. Parker, J. Peiró, S.M. Byrd, S.J. Sherwin: "Modelling the circle of Willis to assess the effects of anatomical variations and occlusions on cerebral flows". *J. Biomech.*, vol. 40, no. 8, 2007, pp. 1794 -1805.

[5] F. Cassot, V. Vergeur, P. Bossuet, B. Hillen, M. Zagzoule, J.P. Marc-Vergnes: "Effects of anterior communicating artery diameter on cerebral hemodynamics in internal carotid artery disease. A model study". *Circulation*, vol. 92, no. 10, Nov 1995, pp. 3122-3131.

[6] B. Hillen, H.W. Hoogstraten, L. Post: "A mathematical model of the flow in the circle of Willis". *Biomech.*, vol. 19, no. 3, 1986, pp. 187-194.

[7] A. Ferrández, T. David, M.D. Brown: "Numerical models of auto-regulation and blood flow in the cerebral circulation". *Comput Methods Biomech Biomed Engin*, vol. 5, no. 1, Feb. 2002, pp. 7-19.

[8] S.M. Moore, K.T. Moorhead, J.G. Chase, T. David, J. Fink: "One-dimensional and three-dimensional models of cerebrovascular flow". *J Biomech Eng*, vol. 127, no. 3, Jun. 2005, pp. 440-449.

[9] S.M. Moore, T. David, J.G. Chase, J. Arnold, J. Fink: "3D models of blood flow in the cerebral vasculature". *J Biomech*, vol. 39, no. 8, 2006, pp. 1454-1463.

[10] N. Westerhof, N. Stergiopulos: "Models of the arterial tree". *Stud Health Technol Inform*, 2000, vol. 71, pp. 65-77.

[11] M. Schwarz, M.P. Nguyen, U. Kiencke, C. Heilmann, R. Klemm, C. Benk, F. Beyersdorf, H.J. Busch: "Integration of the Circle of Willis into Avolio's Model of the Arterial Haemodynamics". *Proceedings of the Sixth IASTED International Conference on Biomedical Engineering*, Innsbruck, Austria, 2008, pp. 193-198.

[12] R. Prêtre, M.I. Turina: *Deep Hypothermic Circulatory Arrest*. vol. 2, 2003, pp. 401-412.

[13] H. Stephan: *Cerebral effects of hypothermic extracorporeal circulation*. Springer-Verlag, 1991. (in German)

[14] M. Karamanoglu, D.E. Gallagher, A.P. Avolio, M.F. O'Rourke: "Functional origin of reflected pressure waves in a multibranched model of the human arterial system". *Am J Physiol*, vol. 267, no. 5, Pt 2, Nov. 1994, pp. H1681-H1688.

[15] E. Naujokat, U. Kiencke: "Observation of the patient's state in cardiac surgery". vol. 50 no. 5, pp. 204–211, 2002. (in German)

[16] M.C. Lewis: "Hypothermia". *Anesthesiology Online*, 1998.

[17] D.W. Newell, R. Aaslid, A. Lam, T.S. Mayberg, H.R. Winn: "Comparison of flow and velocity during dynamic autoregulation testing in humans". *Stroke*, vol. 25, no. 4, Apr. 1994, pp. 793-797.

[18] K.T. Moorhead, C.V. Doran, J.G. Chase, T. David: "Lumped parameter and feedback control models of the auto-regulatory response in the Circle of Willis". *Comput Methods Biomech Biomed Engin*, vol. 7, no. 3, Jun. 2004, pp. 121-130.

[19] K.T. Moorhead, J.G. Chase, T. David, J. Arnold: "Metabolic model of autoregulation in the Circle of Willis". *J Biomech Eng*, vol. 128, no. 3, Jun 2006, pp. 462-466.

[20] A.C. Guyton, J.E. Hall: *Textbook of medical physiology*. Saunders, 1996.

[21] S. Silbernagl, A. Despopoulos: *Pocket atlas of physiology*. 1991. (in German)

[22] A.M. Grigore, L.Jr. Brusco: "Temperature regulation and manipulation during surgery and anesthesia". *Anesthesiology Online Journal*, vol. 5, 1998.

[23] A. Kurz, D.I. Sessler, F. Birnbauer, U.M. Illievich, C.K. Spiss: "Thermoregulatory vasoconstriction impairs active core cooling". *Anesthesiology*, vol. 82, no. 4, Apr 1995, pp. 870-876.

[24] D. Fiala, K.J. Lomas, M. Stohrer: "A computer model of human thermoregulation for a wide range of environmental conditions: the passive system". *J Appl Physiol*, vol. 87, no. 5, Nov. 1999, pp. 1957-1972.

[25] R.G. Gordon, R.B. Roemer, S.M. Horvath: "A Mathematical Model of the Human Temperature Regulatory System – Transient Cold Exposure Response". *IEEE Transactions on Biomedical Engineering*, vol. 23, no. 6, 1976, pp. 434-444.

[26] J.A.J. Stolwijk, J.D. Hardy: "Temperature regulation in man – a theoretical study". *Pflügers Arch Gesamte Physiol Menschen Tiere*, vol. 291, no. 2, 1966, pp. 129-162.

[27] X. Xu, J. Werner: "A Dynamic Model of the Human/Clothing/Environment-System". *Appl Human Sci*, vol. 46, no. 2, 1997, pp. 61-75.

[28] F.B. Sachse, C.D. Werner, M. Müller, K. Meyer-Waarden: "Preprocessing of the Visible Man dataset for the generation of macroscopic anatomical models". *Proc. First Users Conference of the National Library of Medicine's Visible Human Project*, 1996.

[29] F.B. Sachse, M. Glas, M. Müller, K. Meyer-Waarden: "Segmentation and tissue-classification of the Visible Man dataset using the computertomographic scans and the thin-section photos". *Proc. First Users Conference of the National Library of Medicine's Visible Human Project*, 1996.

[30] D. Fiala, K.J. Lomas, M. Stohrer: "Computer prediction of human thermoregulatory and temperature responses to a wide range of environmental conditions". *Int J Biometeorol*, vol. 45, no. 3, Sep. 2001, pp. 143-159.